Materials Science and Engineering C 33 (2013) 405–410

Contents lists available at SciVerse ScienceDirect

Materials Science and Engineering C

journal homepage: www.elsevier.com/locate/msec

Bone fracture characterization using the end notched flexure test

N. Dourado [a,*], F.A.M. Pereira [a,b], M.F.S.F. de Moura [b], J.J.L. Morais [a], M.I.R. Dias [c]

[a] CITAB/UTAD, Departamento de Engenharias, Quinta de Prados, 5001-801 Vila Real, Portugal
[b] Faculdade de Engenharia da Universidade do Porto, Departamento de Engenharia Mecânica, Rua Dr. Roberto Frias, 4200-465 Porto, Portugal
[c] UTAD, Departamento de Ciências Veterinárias, Quinta de Prados, 5001-801 Vila Real, Portugal

ARTICLE INFO

Article history:
Received 15 February 2012
Received in revised form 20 August 2012
Accepted 17 September 2012
Available online 24 September 2012

Keywords:
Bone
Mode II
Fracture characterization
End notched flexure test
Cohesive zone modeling

ABSTRACT

A miniaturized version of the end notch flexure test was used in the context of pure mode II fracture characterization of bovine cortical bone. To overcome the difficulties intrinsic to crack length monitoring during its propagation an equivalent crack method was employed as data reduction scheme. The proposed method was validated numerically by means of a finite element analysis including a cohesive zone modeling and subsequently applied to experimental results to determine the fracture energy of bone under pure mode II loading. Finally, a cohesive law representative of fracture behavior of each specimen was determined employing an inverse method, considering a trapezoidal shape for the softening law. The consistency of the obtained results leads to the conclusion that the trapezoidal law is adequate to simulate fracture behavior of bone under mode II loading. The proposed testing setup and the employed data reduction scheme constitute powerful tools in which concerns fracture characterization of bone under pure mode II loading and can be viewed as the main outcomes of this work.

1. Introduction

Bone is a natural composite material, organized on a multi-scale hierarchical structure and constituted by collagen, water and mineral (hydroxyapatite) phase. The arrangement of these components in bone leads to a light and tough structure that is efficient and adapted to sustain complex mechanical loadings. However, fracture risks induced by diseases, drugs, age and accidents constitute fundamental issues which deserve special attention. In this context, the evaluation of bone toughness and respective fracture mechanisms arise as crucial research topics to predict and prevent fracture risks in bone. On the other hand, biologically inspired materials can be conceived to replace bone in many applications. Consequently, engineers interested in designing novel biologically-inspired materials should have appropriate methodologies to characterize fracture of the referred materials.

Fracture studies found in the literature are predominantly dedicated to mode I fracture [1–4]. However, a considerable number of fractures in bone are induced by shear loading, which occurs during torsion and twisting efforts. Furthermore, fracture under pure mode II loading has been attracting much less attention of the research community owing to experimental difficulties inherent to definition of a proper test method. Classical experimental tests used in the context of mode II fracture characterization of materials, as is the case of the end notched flexure (ENF), end load split (ELS) and four-point end-notched flexure (4-ENF) require specimen dimensions impossible to get in bone. To date only three different experimental methods have been proposed in the literature to characterize bone fracture under pure mode II loading. Norman et al. [5] have used the compact shear test which consists on loading in shear a specimen similar to the well known compact tension test (CT). However, some difficulties were pointed to this test. One of them is the nearly insensibility of compliance as a function of crack length, which renders difficult the establishment of compliance calibration that is habitually used to estimate material toughness. Additionally, unstable crack propagation and a quite short ligament length hinder a correct evaluation of fracture energy under pure mode II loading [6]. Zimmermann et al. [7,8] utilized the asymmetric four-point bending test using single edge notched specimens to fracture characterization of bone under mixed-mode I + II loading. Mode II loading is a particular case only achieved when the pre-crack is oriented along the centerline of the rig. In fact, in this situation the bending moment cancels and a shear force is present. However, posterior numerical analyses of this test [6] have shown that fracture process zone ahead of the crack tip is under mixed-mode I + II instead of the intended pure mode II, which leads to a monotonic increase of the *R*-curve as the crack grows. Recently, de Moura et al. [9] performed a numerical analysis on the application of the ELS and ENF tests to pure mode II fracture characterization of bone. The main concerns were related to specimen dimensions available in bone versus extensive fracture process zone that develops under pure mode II loading. Effectively, it must be guaranteed that self-similar crack growth occurs for a given crack extent in order to provide a valuable measurement of fracture energy. The authors have concluded that with a careful choice of specimen dimensions, both tests (ELS and ENF) can be used to measure pure mode II toughness in bone. More recently, the same authors [6] carried out experimental

* Corresponding author. Tel./fax: +351 259 350 356.
E-mail address: nunodou@gmail.com (N. Dourado).

0928-4931/$ – see front matter © 2012 Elsevier B.V. All rights reserved.
http://dx.doi.org/10.1016/j.msec.2012.09.006

ELS tests using bovine cortical bone. They verified that the ELS test is adequate for this purpose, although some aspects rendering this test less attractive may be pointed. One of them is the variability of the clamping conditions which influences the measured toughness, as thoroughly discussed in de Moura et al. [9]. As a consequence of this issue and of the observed scattering in the elastic modulus typical of natural materials, it is necessary to perform previous measurement of this property for each specimen before execution of the fracture test. The ENF test does not present the referred limitations, although it provides a smaller region for self-similar crack growth as discussed in de Moura et al. [9].

As a result of the aspects discussed above, the adequacy of the ENF test to mode II fracture characterization of young bovine cortical bone is evaluated experimentally in this work. Owing to specimen size limitations, a miniaturized testing device was conceived. Furthermore, an equivalent crack length method was pursued due to difficulties intrinsic to crack monitoring during its propagation. The method is based on beam theory and specimen compliance to obtain the *R*-curve, whose plateau defines the critical fracture energy. Cohesive zone modeling (CZM) was used to validate numerically the proposed approach. The data reduction method was applied to experimental results in order to evaluate mode II bone toughness. A trapezoidal cohesive law was determined for each specimen by means of an inverse method involving a fitting procedure between numerical and experimental load–displacement curves. The parameters defining the trapezoidal cohesive law for each specimen were derived for bovine cortical bone considering pure mode II loading. In general, consistent laws were obtained, thus proving that the adopted trapezoidal shape adequately represents the pure mode II fracture behavior of bovine bone. It was concluded that the proposed test (ENF), data reduction method and cohesive law estimation propitiate straightforward and appropriate procedures to perform fracture characterization of bone under pure mode II loading.

2. Experiments

Fresh femurs of young bovine were used in the experiments as the testing material. After harvesting, bone was preserved in physiological saline at −20 °C. Bone can be viewed as an orthotropic material with three different directions: the longitudinal direction (L) aligned with osteons, the radial (R) in the thickness direction and the tangential direction (T), as represented in Fig. 1. Specimens were oriented in the longitudinal (L) direction to provide fracture characterization in the TL system, being the first letter the normal direction to the crack plane, and the second one the direction of crack growth (Fig. 1a). Seven ENF specimens were prepared to comply with the nominal dimensions presented in Fig. 1b.

Specimens were harvested from the femur diaphysis (Fig. 1a), which presents unavoidable size limitations. In fact, owing to femur curvature, barely a limited region is available for specimen fabrication to comply with the intended material orientation, thus resulting in maximum nominal length of $2L_1 = 65$ mm and height $2h = 6$ mm. As a consequence, the span length ($2L$ in Fig. 1b) is limited to 60 mm.

Fracture experiments in bone involving the ENF test revealed that crack frequently deviates from its initial plane (i.e., $z = 0$ in Fig. 1b). Therefore, two slight longitudinal grooves were executed along the longitudinal direction in both lateral sides, leading to a cross section nominal width $b = 2.3$ mm in the crack plane, instead of $B = 3.3$ mm (Fig. 1b). This procedure has been performed by means of a milling operation using a ceramic abrasive material.

Such procedure induced crack propagation along the specimen mid-plane, thus avoiding mixed-mode loading instead of the intended pure mode II loading. The initial crack length a_0 is formed by a notch (0.3 mm thick) fabricated with a circular saw and a natural short crack with 0.25 mm nominal length, executed using a sharp blade. This procedure avoids unwanted blunt cracks which cause a spurious

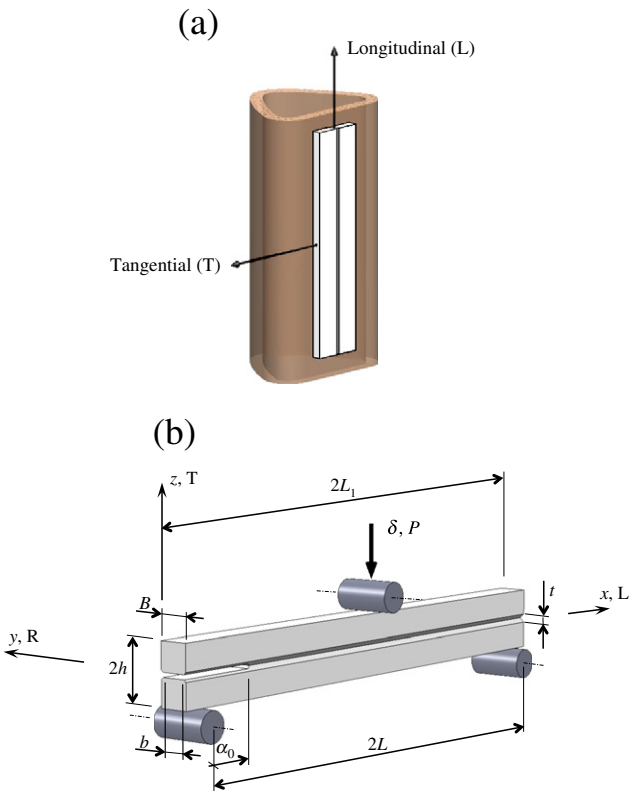

Fig. 1. Representation of (a) a femur segment showing the position and orientation of the specimen and (b) the ENF testing setup ($2L_1 = 65$; $2L = 60$; $2h = 6$; $t = 1$; $B = 3.3$; $b = 2.3$; $a_0 = 21$ mm).

increase of fracture energy at crack initiation (visible in the *R*-curve) as observed by Morais et al. [4]. In order to induce stable crack propagation, the initial crack had a length a_0 equal to 70% of the specimen half-length L [10], which means that a nominal value of $a_0 = 21$ mm was considered.

Load–displacement curves (P–δ curves) were obtained using a servo-electrical testing system (MicroTester INSTRON 5848), with constant displacement rate of 0.5 mm/min. A 2 kN load-cell was used, and the data acquisition frequency was set equal to 5 Hz. Fig. 2 illustrates the testing setup of the performed ENF tests. In order to minimize spurious friction effects, two Teflon® films with a pellicle of lubricant between them were introduced in the pre-crack region (Fig. 2). Fig. 3 (Detail A) puts into evidence the relative shear displacement at the notch tip proving the existence of sliding, characteristic of mode II loading. It is also evident that the crack-tip position is not easily identified with accuracy in this test (Fig. 3 — Detail B). Effectively, under mode II loading crack tends to propagate closed, which precludes the clear identification of its length in the course of the fracture test.

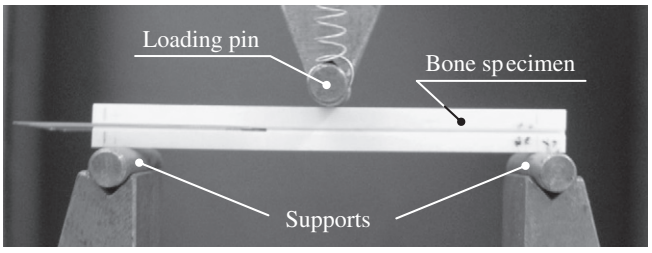

Fig. 2. Testing setup of the ENF test.

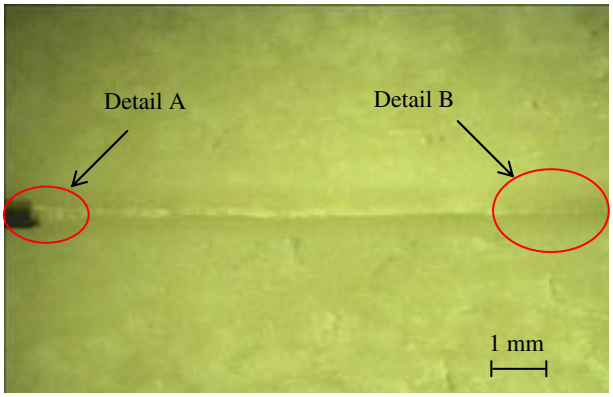

Fig. 3. Shear displacement at the notch tip (detail A) and undefined crack tip position (detail B).

Fig. 4 shows different surfaces observed by SEM (Philips-FEI Quanta 400) in a tested ENF bone specimen. Region A shows the typical pre-crack surface initiated by the saw and adjusted by a sharp blade (region B). Lateral grooves are identified by regions C. The transition between the pre-crack and mode II propagation surface (region D) is clearly visible in this SEM image. Fig. 5 shows in more detail the fractured surface originated by mode II crack propagation (region D in Fig. 4). It can be seen that the surface is in general rough and irregular which is explained by the internal bone microstructure. It is known that cortical bone of young bovines has a plexiform microstructure, with alternate layers of woven bone and lamellar bone [11]. The vascular canals form a two-dimensional network in the middle of each lamellar bone layer, or are more irregularly disposed with the associated primary osteons. As a consequence of this microstructure, material heterogeneity arises, thus leading to several mode II bone failure mechanisms. The observed uneven surface in Fig. 5 is responsible for the increase of fracture energy during crack propagation and is mainly caused by deflections in crack path. Dissipation of energy also occurs by means of micro-crack formation. Additionally, at the sub-microstructural level toughening mechanisms like molecular uncoiling, intermolecular and fibrillar sliding also contribute to increase material toughness [12]. Moreover, surface roughness is responsible for friction due to sliding between fractured surfaces in the course of mode II test, which dissipates additional energy.

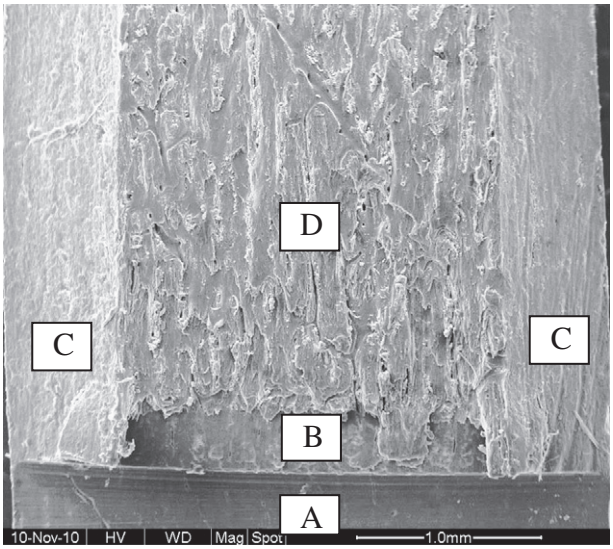

Fig. 4. Fracture surface: A — initial notch; B — pre-crack using a blade; C — lateral grooves; D — mode II fracture surface.

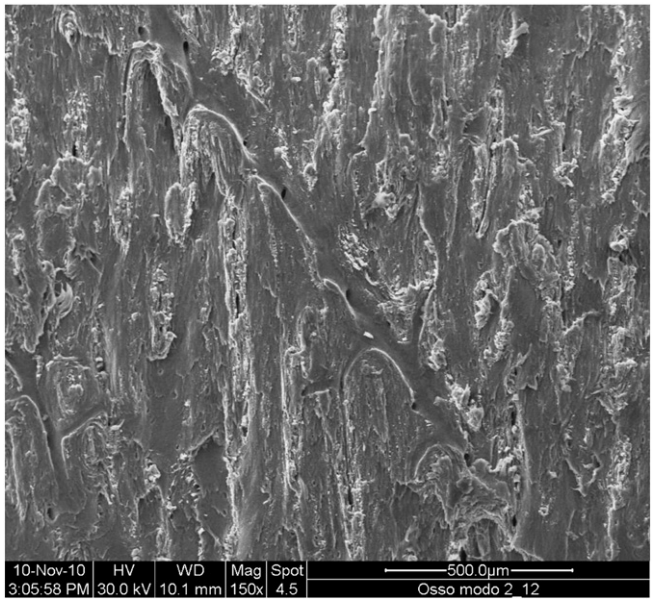

Fig. 5. Detail of fracture surface — region D in Fig. 4.

The described damaging processes occur in part ahead of the crack tip leading to a non-negligible FPZ, which is responsible for a considerable amount of energy dissipation during fracture propagation. An inevitable consequence is the difficulty to distinguish the FPZ from the clear crack, which aggravates the already referred problems on the identification of crack tip. To solve this inconvenience an equivalent crack method presented in the next section is used to evaluate *R*-curves corresponding to mode II loading in bone.

3. Compliance based beam method

The relationship between specimen compliance ($C=\delta/P$) and crack length (a) can be established through Timoshenko beam theory [13],

$$C=\frac{3a^3+2L^3}{8Bh^3E_L}+\frac{3L}{10BhG_{LT}} \tag{1}$$

with E_L and G_{LT} standing for the elastic longitudinal and shear moduli, respectively. There are some aspects that can affect the accuracy of Eq. (1) when applied to the present case. Effectively, crack tip root rotation and stress concentration are not accounted for when beam theory is considered. Additionally, bone is a natural material presenting a pronounced scatter in its elastic properties. These aspects can be indirectly taken into account by means of a corrected elastic modulus E_f obtained from Eq. (1) using the initial values of crack length (a_0) and compliance (C_0),

$$E_f=\frac{3a_0^3+2L^3}{8Bh^3}\left(C_0-\frac{3L}{10BhG_{LT}}\right)^{-1}. \tag{2}$$

Table 1
Elastic properties of bovine cortical bone [4,14].

E_L (GPa)	E_T (GPa)	G_{LT} (GPa)	ν_{LT}
19.94	11.7	4.1	0.36

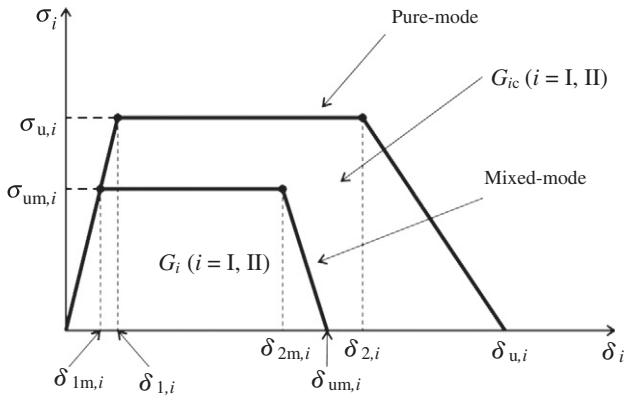

Fig. 6. Trapezoidal stress–displacement law for pure and mixed-mode loading.

During crack growth the current compliance C is used to estimate an equivalent crack length a_e through Eqs. (1) and (2),

$$a_e = \left[\frac{C_c}{C_{0c}}a_0^3 + \frac{2}{3}\left(\frac{C_c}{C_{0c}} - 1\right)L^3\right]^{1/3} \tag{3}$$

where

$$C_c = C - \frac{3L}{10BhG_{LT}};\; C_{0c} = C_0 - \frac{3L}{10BhG_{LT}}. \tag{4}$$

Using Eqs. (1) and (3), and Irwin–Kies relation,

$$G_{II} = \frac{P^2}{2b}\frac{dC}{da} \tag{5}$$

$G_{II} = f(a_e)$ can be obtained as

$$G_{II} = \frac{9P^2a_e^2}{16bBh^3E_f}. \tag{6}$$

It should be referred that the width of the ligament section is affected by the presence of the longitudinal grooves. Consequently, in Eq. (5) the parameter b is used instead of B, which represents the specimen width (Fig. 1).

Eq. (6) allows obtaining the R-curve without monitoring the crack length a during propagation, which is an almost impossible task to perform accurately in mode II fracture characterization tests. Therefore, according to this analytical procedure, the unique required material property is G_{LT}. However, it was verified in previous studies [6] that a typical value of G_{LT} can be used (Table 1), since the measured G_{IIc} is not remarkably influenced for a wide range of G_{LT} values.

4. Model validation

In order to verify if the procedure propitiates a rigorous measurement of the actual mode II toughness, a numerical validation of the ENF test was performed using the finite element method (FEM) and including the trapezoidal CZM described in the following section.

4.1. Trapezoidal CZM

A trapezoidal cohesive zone model (CZM) was used in the numerical analysis to simulate damage onset and growth (Fig. 6). The CZM is based on a constitutive relationship relating stresses ($\boldsymbol{\sigma}$) and relative displacements ($\boldsymbol{\delta}$) between homologous points of the interface elements. Therefore, before damage onset it can be written

$$\boldsymbol{\sigma} = \mathbf{E}\boldsymbol{\delta} \tag{7}$$

where $\mathbf{E}$ is the stiffness diagonal matrix containing the stiffness parameters e_i (i = I, II). These parameters must be defined in order to avoid spurious interpenetrations between the interface element faces and at the same time avoid numerical instabilities. Values in the order of 10^6–10^7 N/mm^3 usually provide a good compromise. Under pure-mode loading, damage onset takes place once stress reaches the local strength $\sigma_{u,i}$, thus defining the corresponding relative displacement $\delta_{1,i}$ (beginning of the plateau region) from which the progressive material softening occurs. The constitutive equation becomes

$$\boldsymbol{\sigma} = (\mathbf{I} - \mathbf{D})\mathbf{E}\boldsymbol{\delta} \tag{8}$$

where $\mathbf{I}$ is the identity matrix and $\mathbf{D}$ is a diagonal matrix containing, on the position corresponding to mode i (i = I, II), the damage parameter. After a certain value of relative displacement ($\delta_{2,i}$) which is defined by material characteristics, stress softening takes place. The ultimate relative displacement corresponding to complete failure ($\delta_{u,i}$) is calculated by equating the area circumscribed by the trapezoid to the respective fracture energy (G_{ic}).

Although a pure mode II fracture characterization is envisaged in this study, in general, bone is under mixed-mode loading. Consequently, a mixed-mode damage model formulation was used (Fig. 6), which obviously includes the pure mode loading cases. Under mixed-mode I + II loading, a quadratic stress criterion is utilized to deal with damage onset

$$\begin{cases} \left(\dfrac{\sigma_I}{\sigma_{u,I}}\right)^2 + \left(\dfrac{\sigma_{II}}{\sigma_{u,II}}\right)^2 = 1 & \text{if } \sigma_I > 0 \\ \sigma_{II} = \sigma_{u,II} & \text{if } \sigma_I \le 0 \end{cases} \tag{9}$$

with σ_i (i = I, II) representing the stresses in each mode. In the previous equation it is stated that normal compressive stresses do not induce damage. Combining Eqs. (7) and (9) for $\sigma_I > 0$, gives

$$\left(\frac{\delta_{1m,I}}{\delta_{1,I}}\right)^2 + \left(\frac{\delta_{1m,II}}{\delta_{1,II}}\right)^2 = 1 \tag{10}$$

where $\delta_{1m,i}$ (i = I, II) represent relative displacements in each mode corresponding to damage onset. A quadratic criterion based on relative

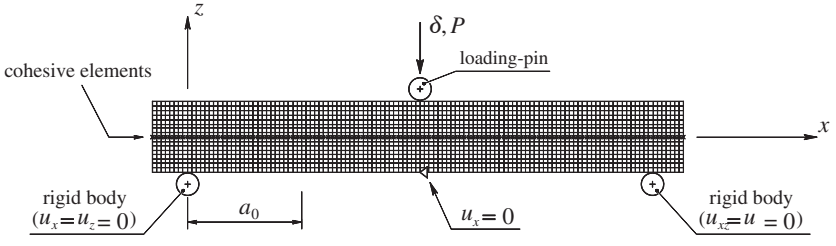

Fig. 7. FEM mesh of the ENF performed in ABAQUS®.

displacements similar to the one expressed in Eq. (10) can be used to define the second inflection point

$$\left(\frac{\delta_{2m,I}}{\delta_{2,I}}\right)^2+\left(\frac{\delta_{2m,II}}{\delta_{2,II}}\right)^2=1 \tag{11}$$

where $\delta_{2m,i}$ (i = I, II) are the relative displacements in each mode corresponding to stress softening onset. The equivalent mixed-mode relative displacements corresponding to damage onset (δ_{1m}), stress softening onset (δ_{2m}) and total failure (δ_{um}) are calculated from the respective components as follows

$$\delta_{jm}=\sqrt{\delta_{jm,I}^2+\delta_{jm,II}^2}\ \text{being}\ j=1,2,u. \tag{12}$$

The linear fracture energetic criterion was considered to simulate damage propagation

$$\frac{G_I}{G_{Ic}}+\frac{G_{II}}{G_{IIc}}=1 \tag{13}$$

where G_i and G_{ic} (i = I, II) are calculated from the area of the minor and major trapezoids, respectively (Fig. 6). This procedure permits establishing the relation between energies and relative displacements, thus leading to the equivalent ultimate relative displacement (δ_{um}) using Eq. (12). The damage parameter can now be obtained for the two steps of the cohesive damage law using the equivalent mixed-mode displacements (δ_{1m}, δ_{2m} and δ_{um}). In the plateau region

$$d_m=1-\frac{\delta_{1m}}{\delta_m} \tag{14}$$

where δ_m is the current equivalent mixed-mode displacement that can be obtained from Eq. (12) using the pure mode components, δ_I and δ_{II}. In the stress softening part of the cohesive law

$$d_m=1-\frac{\delta_{1m}(\delta_{um}-\delta_m)}{\delta_m(\delta_{um}-\delta_{2m})}. \tag{15}$$

Damage propagation can now be easily simulated introducing the damage parameter in the constitutive law (Eq. (8)). More details about the trapezoidal mixed-mode CZM can be found in [15].

4.2. Numerical analysis

A refined mesh (Fig. 7) containing 7680 8-node plane stress solid elements (width B) and 240 6-node cohesive elements (width b) implemented through a previously developed user-subroutine [16,17] was used in order to simulate damage initiation and growth in the ENF test. The different widths considered (i.e., b in cohesive elements and B in solid elements) intend to simulate the presence of the grooves and the respective influence on the fracture process. The pre-crack is simulated by "opened" cohesive elements, which are only able to transmit compressive stresses. In fact, friction effects were neglected due to the use of two thin Teflon® films with a lubricant between them in the experiments. The loading cylinder and supports were simulated as rigid bodies, and contact conditions were considered to transmit the loads. In order to avoid rigid body motion the mid-span node at the bottom specimen edge was constrained in the horizontal direction (Fig. 7). Fracture was induced in the TL system (Fig. 1) through a vertical displacement applied to the central loading-pin. The elastic properties of bovine bone are presented in Table 1. The average value of bovine bone fracture energy under mode II loading (G_{IIc} = 2.65 N/mm) determined in a previous work [6], was used in this numerical analysis.

The R-curve resulting from the numerical simulation presents an excellent agreement on its plateau with the inputted fracture energy G_{IIc} (Fig. 8). This result proves that the proposed data reduction scheme (Section 3) is able to capture the actual G_{IIc}. Consequently, the proposed procedure will be applied in the next section to experimental results.

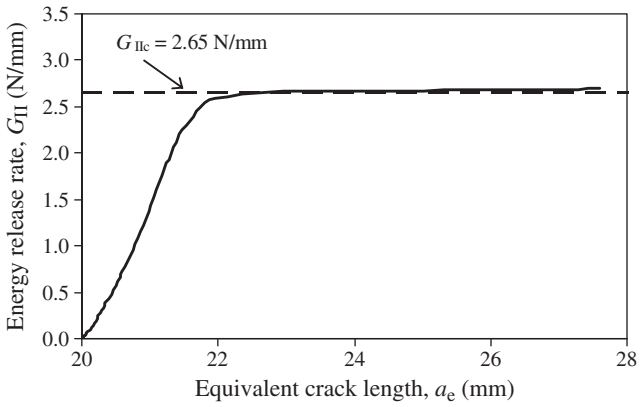

Fig. 8. Numerical R-curve of the ENF test.

5. Results and discussion

A typical load–displacement curve and the corresponding R-curve obtained in the experiments are shown in Fig. 9a and b, respectively. The R-curve obtained by applying the proposed methodology presents an initial ascending branch followed by a plateau and a subsequent ascending part. The first branch corresponds to the FPZ development ahead of the crack tip. Effectively, several damaging processes (e.g., interstitial micro-cracking, cement line debonding and osteons pullout) develop before crack initiation occurs [12]. This effect influences the

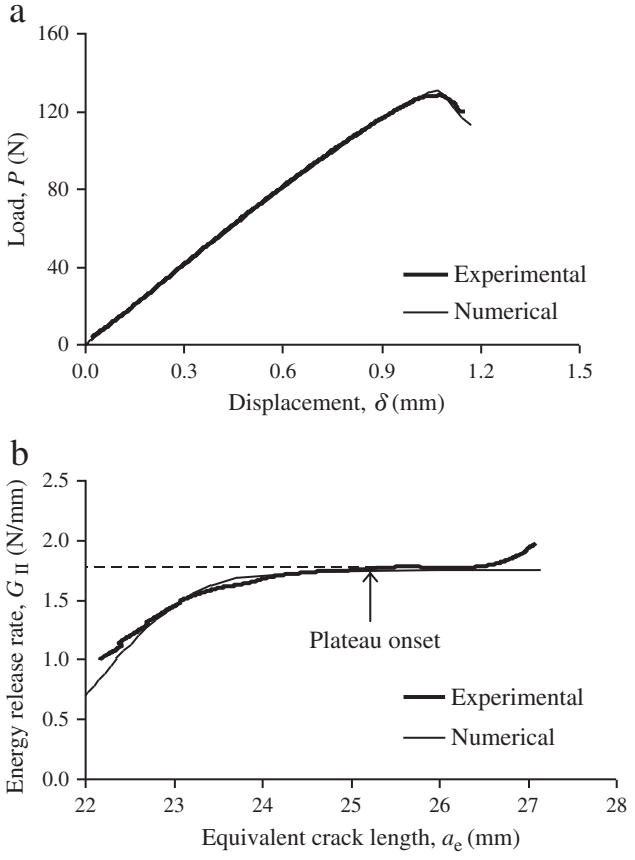

Fig. 9. Typical (a) load–displacement curve and (b) the corresponding R-curve.

Table 2
Resume of experimental results.

Specimen	G_{IIc} (N/mm)	$\sigma_{u,II}$ (MPa)	$\delta_{2,II}$ (mm)
1	2.90	63.0	0.023
2	2.40	65.0	0.02
3	2.32	54.0	0.015
4	1.77	58.0	0.013
5	2.30	57.5	0.021
6	1.95	60.0	0.017
7	2.10	59.0	0.018
Average	2.25	59.5	0.018
CoV (%)	16.2	6.1	19.2

load–displacement curve which presents some nonlinearity before the attainment of the peak load and is reflected on the *R*-curve by means of the increase of G_{II} as a function of the equivalent crack length a_e. This is an expectable result since the a_e and G_{II} are obtained from the current specimen compliance, thus reflecting the non-linearity present on P–δ curve. The plateau region corresponds to self-similar crack growth and has a limited length (approximately 2 mm of a_e) owing to the confinement of the FPZ induced by the central loading cylinder (Fig. 1b). Effectively, when the crack approaches the central loading point, the compressive normal stresses that develop nearby this point affect the natural development of the FPZ. As a result, a spurious increase of the G_{II}, visible in the third ascending part of the *R*-curve takes place (Fig. 9b).

Table 2 summarizes the set of experimental results. For each specimen the value of G_{IIc} was taken from the respective plateau of the *R*-curve. An average value of 2.25 N/mm was obtained with a scatter of 16.2%, which is reasonable for a natural material like bone. It is worth noting that the average value of G_{IIc} (considering the respective scatter) is consistent with the one obtained by Feng et al. [18] (i.e., $G_{IIc}=2.43$ N/mm) and with the one determined using the ELS test (i.e., $G_{IIc}=2.65$ N/mm) [6].

In order to obtain a representative trapezoidal cohesive law (Fig. 6) under mode II loading, a numerical analysis of the ENF test was performed for each specimen, considering its real dimensions and the determined value of G_{IIc}. An inverse method based on successive iterations varying $\sigma_{u,II}$ and $\delta_{2,II}$ in the trapezoidal cohesive law was executed to get the best agreement between the numerical and experimental P–δ curve (see Fig. 9a). The resulting values for $\sigma_{u,II}$ and $\delta_{2,II}$ are listed in Table 2. It should be highlighted that the obtained average local strength under mode II loading is of the same order of the shear strength measured by Turner et al. [19] (i.e., $\sigma_{u,II}=51.6$ MPa), using the Iosipescu shear test. Fig. 10 shows all the cohesive laws obtained for the tested specimens. It can be observed that consistent laws were obtained with one exception. The discrepancies between the laws are predominantly dictated by different fracture energies obtained (scatter of 16.2% in Table 2) due to natural material variability. Consequently, it can be concluded that the trapezoidal cohesive law is adequate to mimic bone fracture under pure mode II loading.

6. Conclusions

In this work, the adequacy of the end notched flexure test to fracture characterization of bovine bone was analyzed. A miniaturized version of the testing setup was developed due to specimen size limitations. In order to overcome the difficulties inherent to crack length monitoring in the course of the loading process, a data reduction scheme based on crack equivalent concept was employed. The method was numerically validated through finite element analysis with cohesive zone modeling and subsequently applied to experimental results obtained in the ENF tests. An inverse method based on the fitting between the numerical and experimental load–displacement curves was utilized to get the trapezoidal cohesive law representative of each tested specimen. The consistency of the obtained cohesive laws demonstrates that the trapezoidal shape is adequate to reproduce fracture behavior of bone under mode II loading. Additionally, it can be concluded that the proposed miniaturized end notched flexure test is appropriate for bone fracture characterization under mode II loading and also very simple to execute.

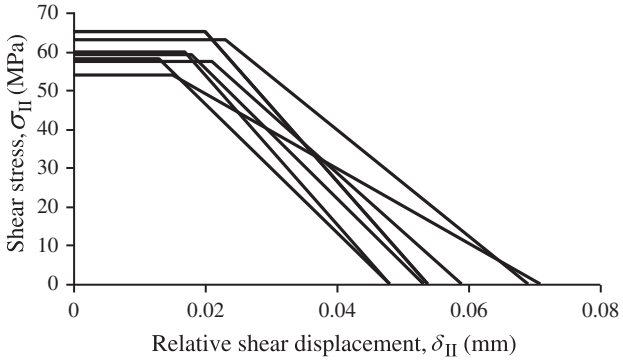

Fig. 10. Trapezoidal cohesive laws obtained using the experimental results.

Acknowledgments

The authors acknowledge the Portuguese Foundation for Science and Technology (FCT) for the conceded financial support through the research project PTDC/EME-PME/119093/2010.

References

[1] T.L. Norman, D. Vashishtht, D.B. Burr, J. Biomech. 28 (1995) 309–320.
[2] J.B. Phelps, G.B. Hubbard, X. Wang, C.M. Agrawal, J. Biomed. Mater. Res. 51 (2000) 735–741.
[3] Q.D. Yang, B.N. Cox, R.K. Nalla, R.O. Ritchie, Bone 38 (2006) 878–887.
[4] J.J.L. Morais, M.F.S.F. de Moura, F.A.M. Pereira, J. Xavier, N. Dourado, M.I.R. Dias, J.M.T. Azevedo, J. Mech. Behav. Biomed. Mater. 3 (2010) 446–453.
[5] T.L. Norman, V. Nivargikar, D.B. Burr, J. Biomech. 29 (1996) 1023–1031.
[6] F.A.M. Pereira, J.J.L. Morais, N. Dourado, M.F.S.F. de Moura, M.I.R. Dias, J. Mech. Behav. Biomed. Mater. 4 (2011) 1764–1773.
[7] E.A. Zimmermann, M.E. Launey, H.D. Barth, R.O. Ritchie, Biomaterials 30 (2009) 5877–5884.
[8] E.A. Zimmermann, M.E. Launey, R.O. Ritchie, Biomaterials 31 (2010) 5297–5305.
[9] M.F.S.F. de Moura, N. Dourado, J.J.L. Morais, F.A.M. Pereira, Fatigue Fract. Eng. Mater. Struct. 34 (2010) 149–158.
[10] L.A. Carlsson, J.W. Gillespie, R.B. Pipes, J. Compos. Mater. 20 (1986) 594–604.
[11] J.D. Currey, Bones: Structure and Mechanics, Princeton University Press, Princeton9780691128047, 2002.
[12] A.R. Najafi, K.P. Saffar, A.R. Arshi, E. Mallakin, H.R. Katouzian, M.R. Eslami, M.H. Moeinzadeh, Akademeia 1 (1) (2011) ea103.
[13] M.F.S.F. de Moura, M.A.L. Silva, A.B. de Morais, J.J.L. Morais, Eng. Fract. Mech. 73 (2006) 978–993.
[14] R.B. Martin, D.B. Burr, N.A. Sharkey, Skeletal Tissue Mechanics, Springer-Verlag, New York0-387-98474-7, 1998.
[15] R.D.S.G. Campilho, M.F.S.F. de Moura, D.A. Ramantani, J.J.L. Morais, J.J.M.S. Domingues, Int. J. Adhes. Adhes. 29 (2009) 678–686.
[16] M.F.S.F. de Moura, J. Adhes. Sci. Technol. 20 (1) (2006) 37–52.
[17] L.M. Durão, M.F.S.F. de Moura, A.T. Marques, Compos. Part A: Appl. Sci. Manuf. 37 (2006) 1325–1333.
[18] Z. Feng, J. Rho, S. Han, I. Ziv, Mater. Sci. Eng. C 11 (2000) 41–46.
[19] C.H. Turner, T. Wang, D.B. Burr, Calcif. Tissue Int. 69 (2001) 373–378.